

# **Experimental study on seismic performance of precast concrete shear walls with defective and repaired grouted sleeve**

Linlin Xie<sup>a, b</sup>, Qiang Liu<sup>a, b</sup>, Xinyu Wang<sup>a, b</sup>, Cantian Yang<sup>a, b \*</sup>

(<sup>a</sup>School of Civil and Transportation Engineering, Beijing University of Civil Engineering and Architecture, Beijing 100044, China;

<sup>b</sup>Multi-Functional Shaking Tables Laboratory, Beijing University of Civil Engineering and Architecture, Beijing 100044, China

**Abstract:** Grouted sleeve connections (GSCs) are widely adopted in precast concrete (PC) shear wall structures. It is critical to reveal the effect of insufficient grouting on the seismic performance of PC shear walls (PSWs), and to recommend as well as validate the repair method for insufficient grouting defects. To achieve this, three full-scale PSWs were tested under cyclic loads: one PSW without grouting defects, one PSW with grouting defect, and one repaired PSW with initial grouting defect. The effects of defect ratio and repair action were analyzed and the test results indicated: 1) bar slip dominated the failure of the specimen with the defect ratio as expected, rather than the flexural failure mode for the specimen without defects. After the occurrence of bar slip, a significant rocking phenomenon was observed, and the damage to concrete was alleviated. The pinching phenomenon was observed for the hysteretic curves, and the strength, deformation, and energy dissipation capacities were significantly lower than those of the specimen without defects, particularly the ductility. 2) The bar-slip behavior was effectively prevented after the repair of the grouting defect, and the repaired specimen exhibited the expected flexural failure mode. The damage evolution mode, strength, deformation capacity, and energy-dissipation capacity were generally comparable with those of the specimen without defects. Rocking behavior and pinching phenomenon were not observed after repair. The negative influences of insufficient grouting were approximately eliminated, thus validating the feasibility and reliability of the repair method.

**Keywords:** full-scale experiment, PC shear wall, grouting sleeve connection, insufficient grouting, defective and repaired grouted sleeve

---

\*Correspondence to: Cantian Yang, School of Civil and Transportation Engineering, Beijing University of Civil Engineering and Architecture, #1 Zhanlanguan Road, Beijing 100044, P.R. China. E-mail: yangcantian@outlook.com

## 1 Introduction

Precast concrete (PC) structures, for example, PC shear wall (PSW) structures and PC frame-shear wall structures, have been widely used to construct residential and public buildings worldwide. The PSW is considered as a critical structural component in these structures, and the seismic performance control of such components is regarded as essential. Grouted sleeve connections (GSCs) have been acknowledged to be effective for ensuring the seismic performance of PC components and structures [4,5]. The corresponding seismic performance is expected to be equivalent to that of cast-in-place reinforced concrete structure [6-8]. However, engineering practices have indicated that insufficient grouting is usually observed because of difficulties in controlling the construction quality [9,10]. It is critical to identify the effect of insufficient grouting on the seismic performance of PSWs [11-13]. Furthermore, a method to detect and repair such defects should be recommended, and the seismic performance of repaired PSWs with initial defects for GSCs needs to be confirmed.

Currently, studies on PSW using GSCs can be divided into two categories: at the GSC level and at the component level. At the GSC level, studies have mostly focused on the influence of insufficient grouting and detection of insufficient grouting for longitudinal rebars with a diameter of 12 to 16 mm, which are usually used for PSW. Ling et al. [14] evaluated the mechanical performance of GSCs with a rebar diameter ( $d$ ) of 16 mm under uniaxial tensile loads, emphasizing the influence of different anchorage lengths and configurations of GSCs. Chen et al. [15] investigated the performance of GSCs with rebar diameters of 12 mm, 14 mm, and 16 mm under large-stress cyclic loads. The effects of three anchorage lengths, including  $8d$ ,  $7d$ , and  $6d$ , were revealed. Zheng et al. [16,17] tested 24 GSCs with a rebar diameter of 16 mm under a uniaxial tensile load and cyclic load, emphasizing the effect of different anchorage lengths. The authors [18,19] also conducted tests of 39 GSCs under uniaxial tensile loads and 13 GSCs under cyclic loads with a rebar diameter of 12 mm, and investigated the influence of insufficient grouting quantified using the defect ratio. All these experimental studies indicated that the insufficient grouting significantly affected the mechanical behavior of GSC, and a bar slip failure mode, instead of a bar fracture failure mode, was observed when the defect ratio reached a relatively large value. This led to poor strength, deformation capacity, and energy dissipation capacity of GSCs. For defect detection of GSCs, non-destructive methods have been recommended and used in real engineering practice, e.g., the X-ray digital imaging technology [20] and ultrasonic time reversal technique [21]. However, concurrent studies on the detection and repair of defective grouted sleeves have rarely been reported. To address this issue, the authors developed a defect-detectable and repairable half-grouted sleeve (DDRHGS) [18], as shown in Fig. 1. An additional hole is introduced to detect and repair insufficient grouting, which is located in the upper part of the outlet of the traditional grouted sleeve. Through GSC tests, the influence of defect ratio was identified, and the reliability of the repair method was verified because the performance of GSCs after repair was approximately identical to that of GSCs without defects, laying a foundation for further studies on PSWs.

At the component level, Xiao et al. [9] conducted tests on seven PSWs with defective GSCs, and the effects

of different regions with insufficient grouting (i.e., boundary element and wall web) and defect ratio were investigated. It is notable that the bar-slip phenomenon that occurred for GSC was not observed at the component level. Through numerical simulation, the uncertainties of the numbers and locations of insufficient grouting were considered for PSW using GSCs by Cao et al. [22]. The influence of insufficient grouting on the seismic performance of the PSW and PC frame-shear wall structures was evaluated. The above literature review indicated that the influence of defective GSCs on the seismic performance of PSW remains rare. Furthermore, inconsistencies existed between the damage modes of the GSC at the connection level and the component level, it is necessary to further identify the relationship between the connection performance of GSC and the seismic performance of PSW using GSC. Meanwhile, investigations on the repair method for PSW using GSCs with insufficient grouting have been rarely reported. Therefore, two issues must be considered carefully. First, the tests of GSCs and PSW are preferred to be concurrently conducted, and the test results of GSCs can provide reference defect ratios for the PSW test. The second issue is the investigation of the seismic performance of a repaired PSW with initial defective GSCs.

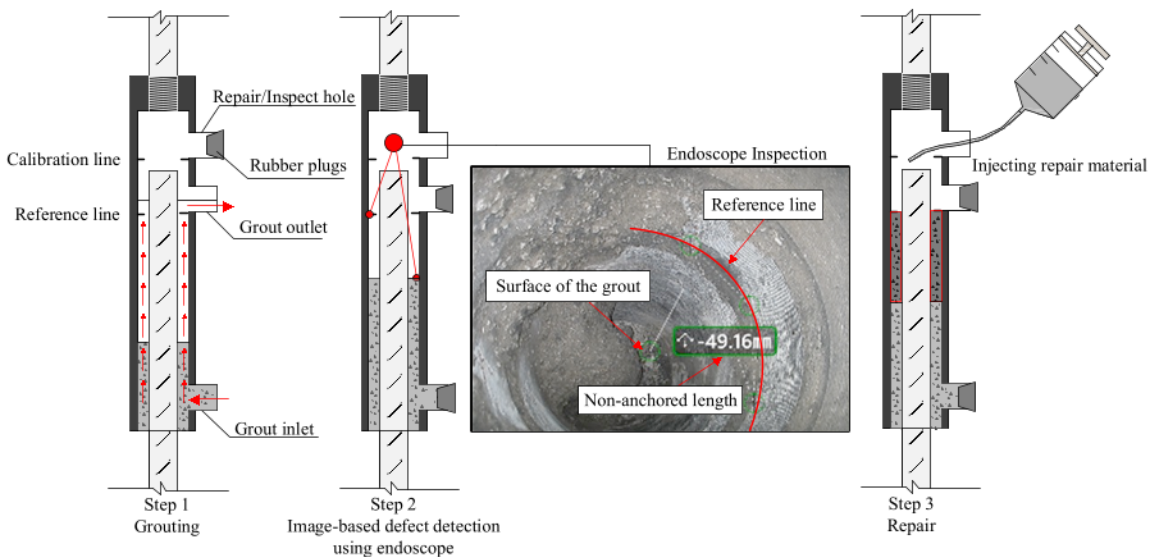


**Fig. 1. Defect detectable and repairable half-grouted sleeve**

To address these issues, three full-scale PSWs using GSCs were tested under cyclic loads, including one PSW without grouting defects, one PSW with a defect ratio of 60% for all GSCs, which was determined by previously cyclic test results of GSCs using identical rebars, and one PSW that initially had a defect ratio of 60%. It is worth mentioning here that the defect ratio of 60% was determined according to the GSC tests conducted by the authors [19] with a diameter of 12 mm, which adopted identical longitudinal rebars, grouted sleeve, and grouting material. A bar-slip failure mode was observed for GSCs with such a defect ratio, and it is also expected to have a certain effect on the seismic performance of PSWs. Through a comparison with PSW without insufficient grouting, the effect of defect ratio on the seismic performance of the PSW with defective GSCs was identified, emphasizing the damage characteristics of defective GSCs. The feasibility and reliability of the repair method were validated through a comparison of the seismic performance of the PSW without insufficient grouting and repaired PSW. The outcome of this study can serve as a reference for quality control

of PSWs using GSCs.

## 2 Experimental programs

### 2.1 Specimens and materials

To reveal the effect of the defect ratio on the seismic performance of PSW and validate the reliability of the repair method for PSW, three full-scale PSWs connected using grouting sleeves were prefabricated and tested under a pseudo-static load, including one PSW without grouting defects (PSW1-0), one PSW with a defect ratio of 60% (PSW2-60), and a repaired PSW with an initial defect ratio of 60% (PSW3-60-R). This defect ratio is determined according to the results of GSC tests conducted by the authors [19]. Specifically, these tests investigated the influence of five defect ratios on the performance of GSCs under cyclic loads, including 0%, 15%, 30%, 45%, and 60%. Typical failure modes and load-deformation curves of the GSC specimens are presented in Fig.2. Detail information and results of these tests could be found in literature [19]. The results indicated that a bar-slip failure mode, poor ductility, and energy dissipation capacity were only observed for the GSCs with a defect ratio of 60%. Note that the longitudinal rebars of these PSWs also adopted the same rebar in the test of GSCs with a diameter of 12 mm. Hence, only a defect ratio of 60% was considered. The critical information of each PSW is presented in Table 1.

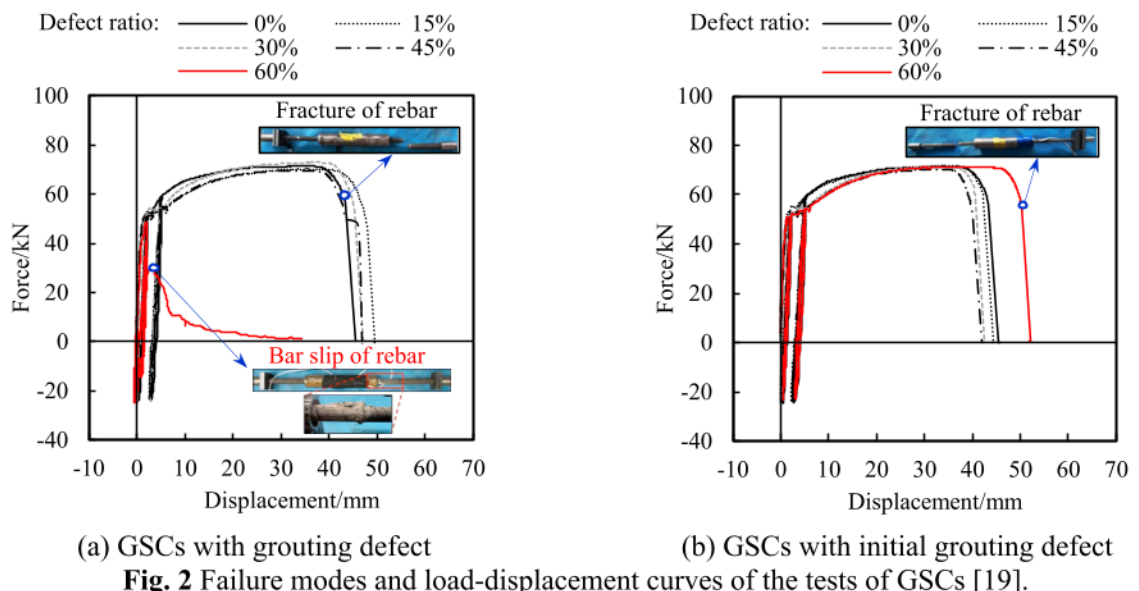


**Fig. 2** Failure modes and load-displacement curves of the tests of GSCs [19].

**Table 1.** Anchoring information of tested specimens

Specimen	Type	$l_h/\text{mm}$	Defect ratio/%
PSW1-0	Specimen without defect	0	0
PSW2-60	Specimen with defect	60	60
PSW3-60-R	Repaired specimen	60→0	60→0

The geometric properties and reinforcement details of the specimens are shown in Fig. 3. The thickness, width, and height from the loading point to the top surface of the foundation of the three specimens were 200

mm, 1800 mm, and 3150 mm, respectively. The longitudinal rebar used was HRB400 with a design yield strength of 400 MPa. To control the defect ratio and facilitate the repair of insufficient grouting, the DDRHGS proposed by the authors was adopted to construct the specimen. The parameters of the DDRHGS are listed in Fig. 4. The defect ratio is defined as  $l_n/l_0$ , where  $l_n$  is the unanchored length of the rebar as shown in Fig. 4,  $l_0$  is the anchorage length required in JGJ 355-2015 [23] ( $l_0$ , approximately eight times the diameter of the rebar).

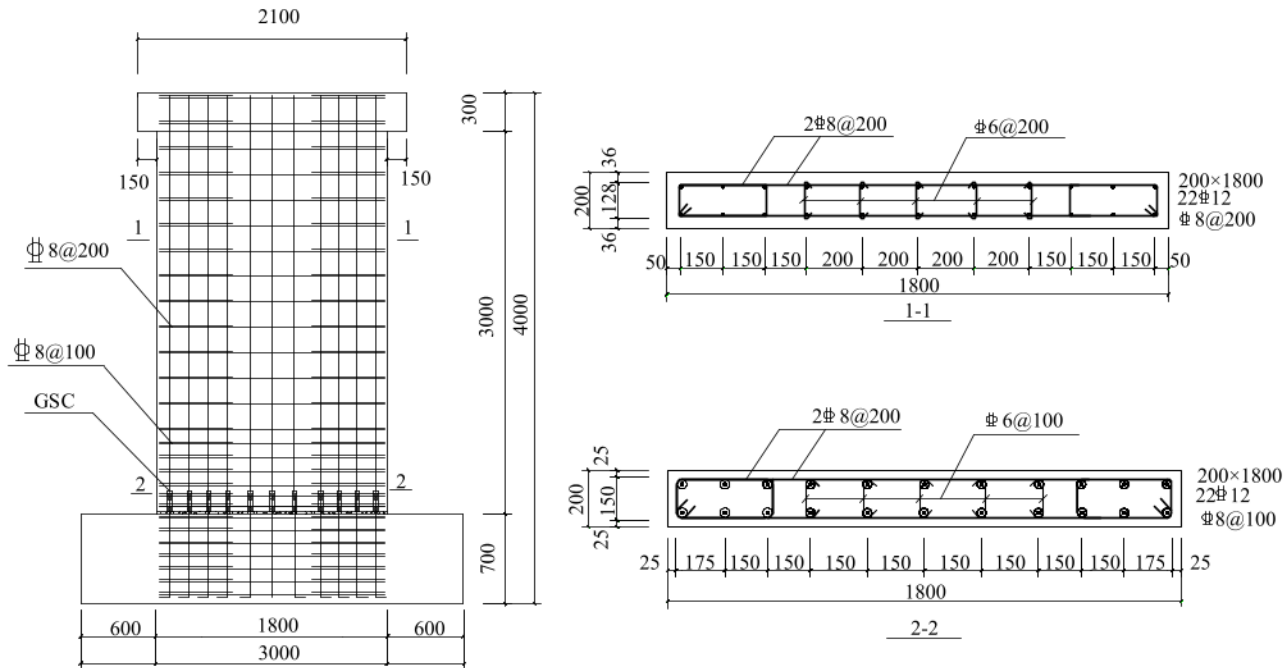


**Fig. 3.** Dimensions and reinforcement details of PC shear walls (Unit: mm)

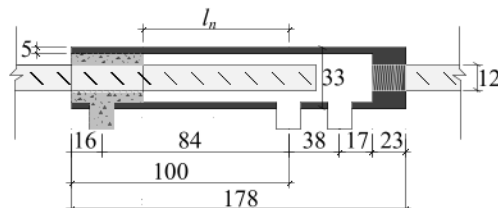


**Fig. 4.** Schematic diagram of DDRHGS (Unit: mm)

PSW1-0 is a reference specimen without grouting defect, that is, the anchorage length is set according to the requirements of the code. PSW2-60 was prefabricated with a defect ratio of 60% by setting an unanchored length of 0.6  $l_0$ . By comparing PSW1-0 and PSW2-60, the effect of the defect ratio on the seismic performance of PSW can be identified. For PSW3-60-R, a specimen identical to PSW2-60 was prefabricated. After 28 days of curing, this defect was repaired through the reinfusion of the grouting material to the state without defect, which is the most unfavorable repair condition, and further cured for 28 days. By comparing PSW3-60-R, PSW1-0, and PSW2-60, the feasibility and reliability of the repair method can be validated for PSWs. The GSC parameters of three specimens are compared in Table 1.

The PC components were cast using C40 concrete, and the tested average cubic strength of six concrete

specimens was 43.52 MPa. The grouting sleeve was made of 45 # structural carbon steel with a yield strength of 335 MPa. The manufacturing process of the specimens is presented in Fig. 5. After grouting, the specimens were cured for 28 days. Subsequently, inspection of the defect ratio was conducted using an endoscope probe (Mentor Visual iQ<sup>TM</sup>[24]). PSW3-60-R was produced through reinfusion to achieve the expected anchorage length and was then maintained for another 28 days. Six prisms of grouting material with sizes of 40 mm × 40 mm × 160 mm were adopted following Chinese code *Cementitious grout for sleeve of rebar splicing* (JG/T 408-2019) [25]. The average compressive strengths of the first and second (for repair) batches of specimens were 87 MPa and 91 MPa, respectively. In addition, the material properties of the rebars are presented in Table 2.



**Fig. 5.** Fabrication of specimens

**Table 2.** Mechanical properties of reinforcements

d/mm	$f_y/\text{MPa}$	$f_u/\text{MPa}$	$E/\text{MPa}$	$\delta/%$
6	592.0	719.0	$2.21 \times 10^5$	11.57
8	455.6	731.3	$1.82 \times 10^5$	11.79
12	506.7	661.7	$1.88 \times 10^5$	12.39

Note:  $f_y$  – yield strength,  $f_u$  – tensile strength,  $E$  – Young's Modulus,  $\delta$  – elongation ratio

## 2.2 Loading protocols and test setup

The test setup presented in Fig. 6 was adopted in this study. An axial load of 1750 kN was vertically applied at the top of the PSWs, and the corresponding designed axial load ratio was 0.25. To facilitate the comparison of the seismic performance of the three specimens under identical deformation levels, especially the damage evolution mode, a displacement control loading protocol was used to apply the horizontal cyclic load, as shown in Fig. 7. Specifically, the loading protocol was divided into three stages, and two cycles were performed at each displacement amplitude according to FEMA 461 [26]. At stage 1, the displacement continuously increased to 10 mm in increments of 2 mm. At stage 2, the displacement continuously increased to 20 mm with an

increment of 5 mm. At stage 3, the displacement continuously increased to 80 mm with an increment of 10 mm.

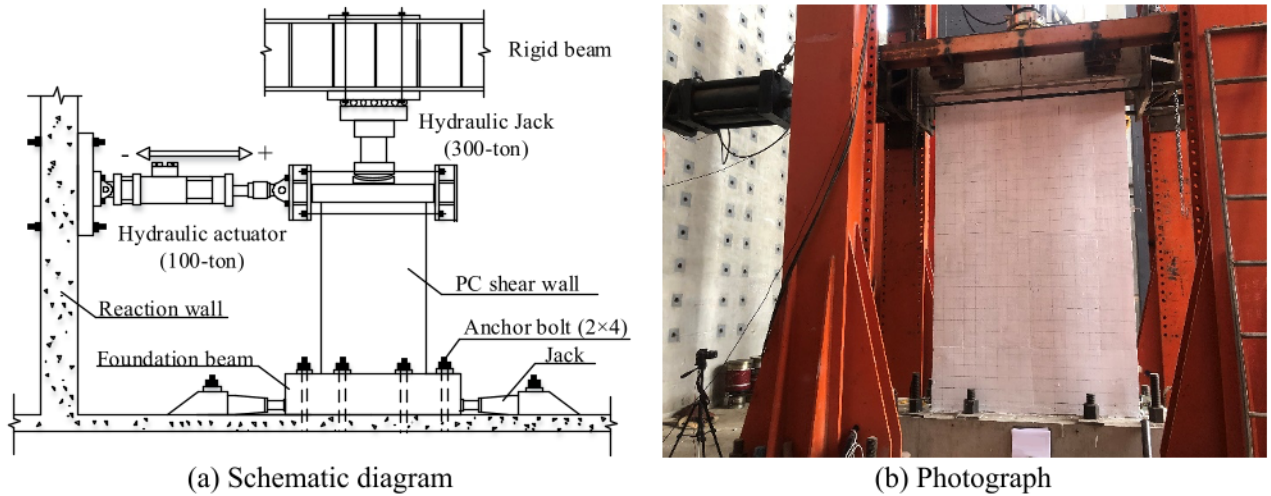


**Fig. 6.** Schematic diagram and photograph of test setup

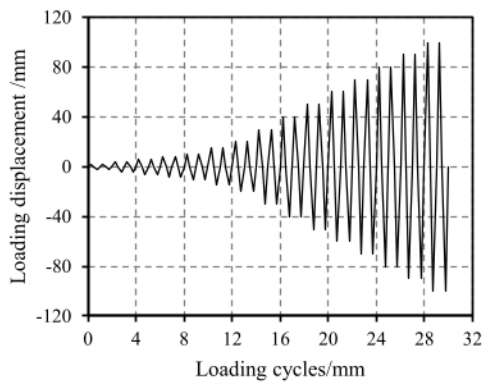


**Fig. 7.** Loading protocol

The measurement scheme is schematically presented in Fig. 8. The horizontal displacements of the points 100 mm, 400 mm, 1000 mm, 1800 mm, and 2600 mm from the top of the foundation were measured using the displacement meters D1, D2, D3, D4, and D5, respectively. The displacement meters D6-1/2 and D7 were arranged to measure the horizontal and out-of-plane displacements of the loading point, respectively. The displacement meter D8 was set to measure the horizontal displacement of the foundation. The displacement meters D11 and D12 were adopted to measure the vertical displacement of the two boundaries of the specimens, while D17 and D18 were set to measure the shear deformation. Because bar slip is expected to occur for the rebar in the GSC with a defect ratio of 60%, vertical displacement meters (D9, D10, D13, D14, D15, and D16) were installed to measure the vertical deformation. All these displacement meters are arranged at the back of the wall as shown in Fig. 8.

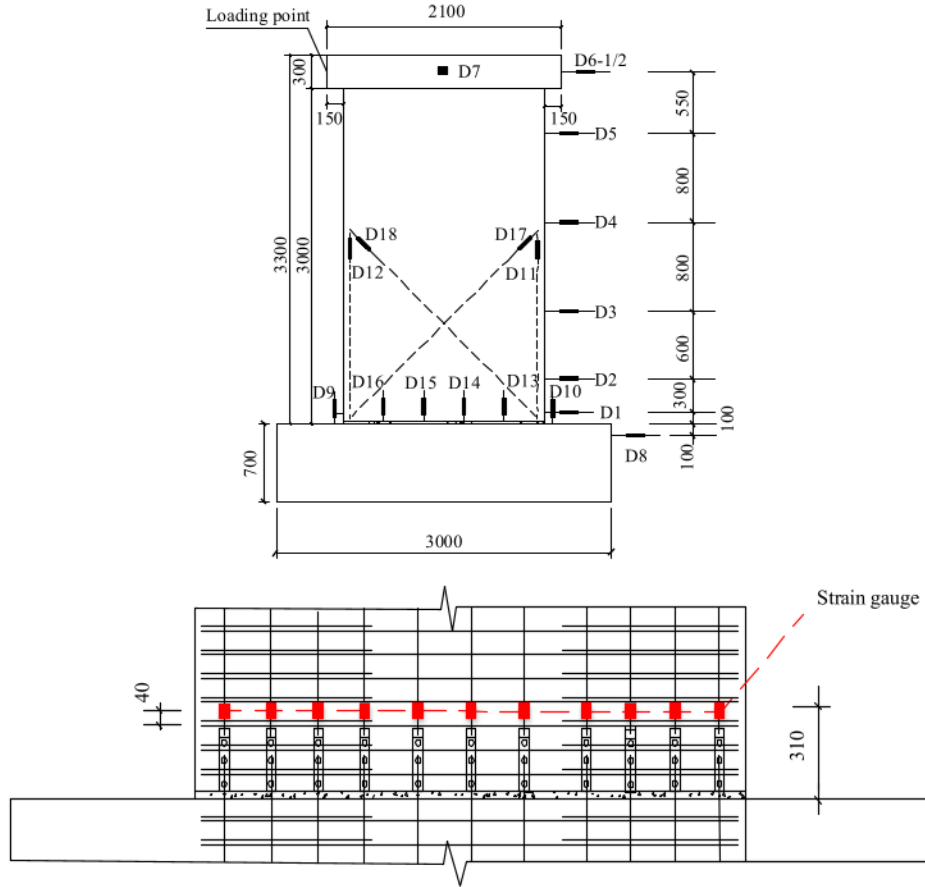


**Fig. 8.** Measurement scheme (Unit: mm)

### 3 Comparison and analyses of test results of PSW1-0 and PSW2-60

#### 3.1 Test phenomena and failure mode

##### 3.1.1 PSW1-0

The flexural behavior dominated the failure of PSW1-0. Photographs of the critical damage states are presented in Fig. 9. The horizontal flexural crack was first observed at the bottom of PSW1-0 with a top displacement of 8 mm (i.e., a drift ratio of 0.254%). As this displacement approached 15 mm (i.e., a drift ratio of 0.476%), the longitudinal rebar yielded and a horizontal flexural crack thorough the section was observed. When the top displacement reached approximately 30 mm (i.e., a drift ratio of 0.952%), the peak load was observed with a value of 754.1 kN associated with the spalling of the cover concrete, as shown in Fig. 9a. At 40 mm (i.e., a drift ratio of 1.270%), numerous flexural-shear diagonal cracks, as shown in Fig. 9b, were observed, and the damage of the concrete in the compressive region became more severe, leading to spalling of the cover concrete within a height of 300 mm from the bottom of PSW1-0. When the top displacement reached 60 mm (i.e., a drift ratio of 1.905%), gap openings of approximately 3 mm and 2 mm were observed at the two edges of the specimen under positive and negative loading, respectively; The value under the positive loading was larger than that under the negative loading because the damage on the right side was more severe than that on the left side. When the top displacement reached 80 mm (i.e., a drift ratio of 2.540%) in the first loading cycle, significant crushing of concrete in the compressive region and buckling of longitudinal rebars were observed as shown in Fig. 9c; thus, the horizontal load decreased to 66.4% of the peak load in the positive direction.

Meanwhile, a gap opening of approximately 4 mm was observed. Subsequently, under negative loading, the buckling rebars fractured, as shown in Fig. 9c, and the horizontal load decreased to 52.9% of the peak load. The test was then terminated, and the gap opening was measured to be approximately 3.8 mm.

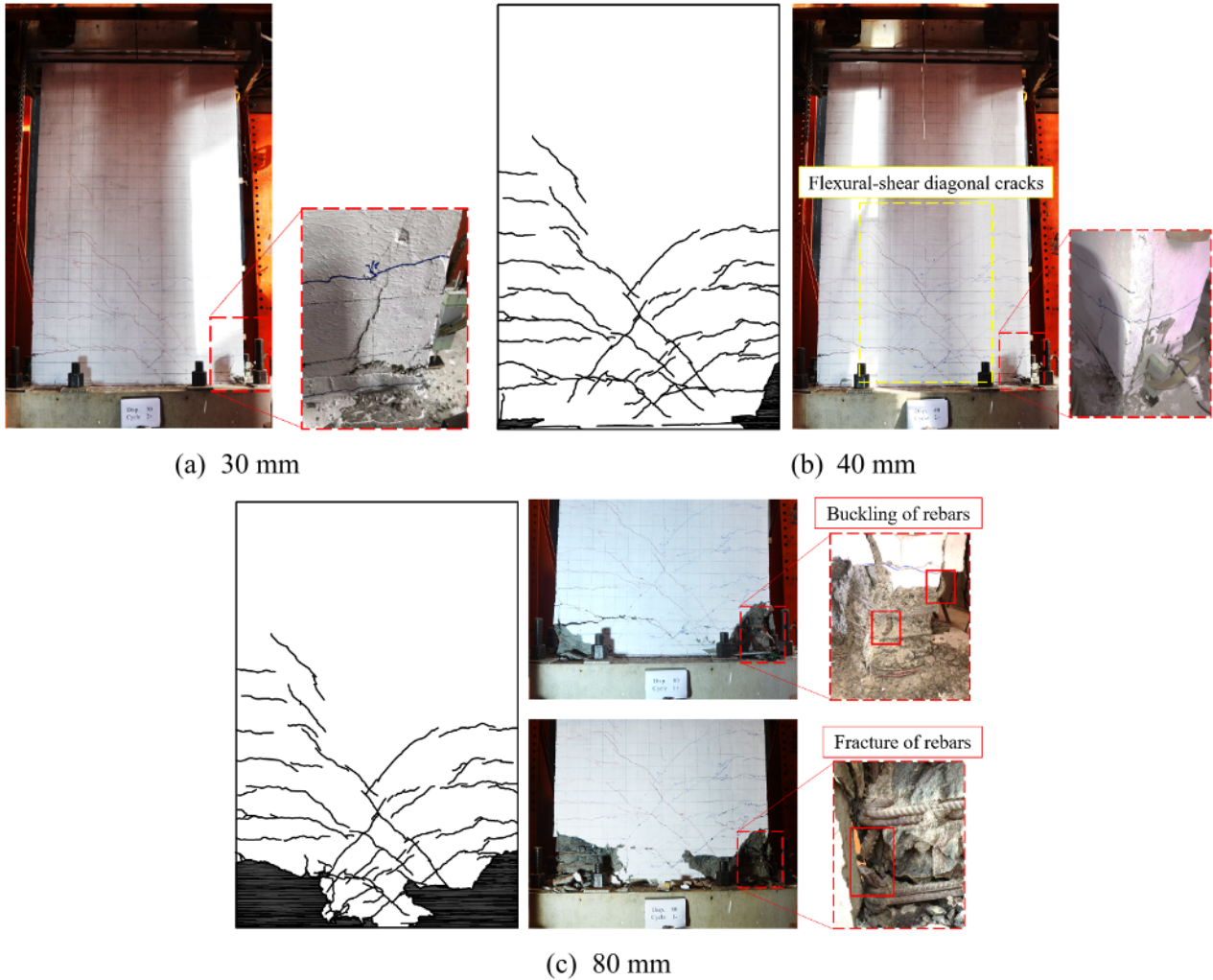


**Fig. 9.** Damage evolution of PSW1-0

### 3.1.2 PSW2-60

For PSW2-60 with a defect ratio of 60%, the expected bar-slip failure mode was observed, which is consistent with the test phenomenon observed in the GSC experiment [19]. Photographs of the critical damage states are presented in Fig. 10. When the top displacement reached 8 mm (i.e., a drift ratio of 0.254%), the first horizontal crack appeared at the bottom of the shear wall. At 15 mm (i.e., a drift ratio of 0.476%), the longitudinal rebar in the boundary element yielded.

The horizontal load reached the peak load 647.4 kN at approximately 20 mm (i.e., a drift ratio of 0.635%) rather than 30 mm for PSW1-0, the peak load is 14.1% lower than that of the specimen without defect (i.e., 754.1 kN for PSW1-0). Meanwhile, at the second loading cycle of 20 mm, the load associated with 20 mm was reduced to 607.5 kN (approximately reduced by 6.2%), such degradation of strength was not observed at the previous displacement amplitude, indicating that the bar slip occurred at 20 mm. Moment-curvature

analysis is conducted to validate that the load degradation is caused by the bar slip of GSC at the drift ratio of 0.635%. Fiber section model in OpenSees [27] is adopted for the moment-curvature analysis, as schematically presented in Fig. 11. Specifically, a ZeroLengthSection element with fiber section is utilized for simulating the section of the shear wall. Geometric and material properties of the fiber section are determined according to the information presented in Section 2. The Steel02 material is adopted to simulate the longitudinal reinforcements. The concrete is simulated using the Concrete01 material. Critical parameters of the strain–stress relationship of the confined and unconfined concrete are determined using the Kent–Scott–Park model [28]. Axial load of 1750 kN is applied to the section. Then, incremental moment load is applied to the section to perform the moment-curvature analysis. During the analysis, strain of the external reinforcing steel fiber (as marked in Fig. 11) is recorded. It is observed that when the curvature of the section reaches 0.635%, the recorded strain of reinforcement is 0.0096, which is 3.57 times of the yield strain of the reinforcement. Such ratio is close to the ratio between the strain corresponding to the bar slip and the strain corresponding to the yielding of rebar of 3.60 as shown in Fig. 2a. Therefore, the load degradation is caused by the bar slip of GSC at the drift ratio of 0.635%.

Subsequently, at the first loading cycle of 30 mm (i.e., a drift ratio of 0.952%) for PSW2-60, anchorage failure of the grouting material occurred and made an obvious sound. A decrease in the horizontal load was observed with a value of 8.4% of the peak load of PSW2-60, which is different from PSW1-0 reaching the peak load. In the second loading cycle, the horizontal load was further reduced by 16.7% of the peak load of PSW2-60, indicating that the bar slip increased further. Meanwhile, gap openings of approximately 7.5 mm (as shown in Fig. 10a) and 5 mm were observed at the two boundaries of the specimen under positive and negative loading, respectively. All these phenomena indicate that significant bar slip occurred at 30 mm. As shown in Fig. 2a, it is notable that the bar slip occurred soon after the yield of the rebar with a diameter of 12 mm when the GSC had a defect ratio of 60%. This is basically consistent with the bar-slip behavior of the longitudinal rebar in PSW2-60, that is, the bar slip occurred soon (i.e., 20 mm) after the yielding of longitudinal rebar (15 mm), and became more severe at 30 mm.

As shown in Fig. 10b, a small number of flexural-shear diagonal cracks were observed with the top displacement reached 40 mm (i.e., a drift ratio of 1.270%). The spalling of cover concrete appeared in a small region. The gap openings of approximately 12.5 mm and 11.5 mm were observed at two boundaries of the specimen under the positive and negative loading, respectively. However, negligible gap openings were observed for PSW1-0 at this top displacement. These are attributed to the fact that the deformation mode of PSW2-60 changed after the occurrence of bar slip, and a certain extent of rocking characteristic with rigid body rotation was observed.

With the continuous increase in the top displacement, an unloading stiffness with a value of approximately zero was observed, that is, a relatively stable load was observed with the decrease in displacement during unloading, which was caused by the bar slip. The stiffness of the specimen increased after the bar slip recovered during the reloading stage. With the top displacement reached 70 mm (i.e., a drift ratio of 2.222%), crushing

of the concrete at the toe of PSW2-60 was observed within a height of 200 mm from the bottom of the shear wall. With the top displacement increased to 80 mm (i.e., a drift ratio of 2.540%), the horizontal load decreased to 78.8% of the peak load. Meanwhile, a gap opening of approximately 27.8 mm was observed, which was significantly larger than that of PSW1-0 at 80 mm (i.e., 4 mm and 3.5 mm at positive and negative loading, respectively).

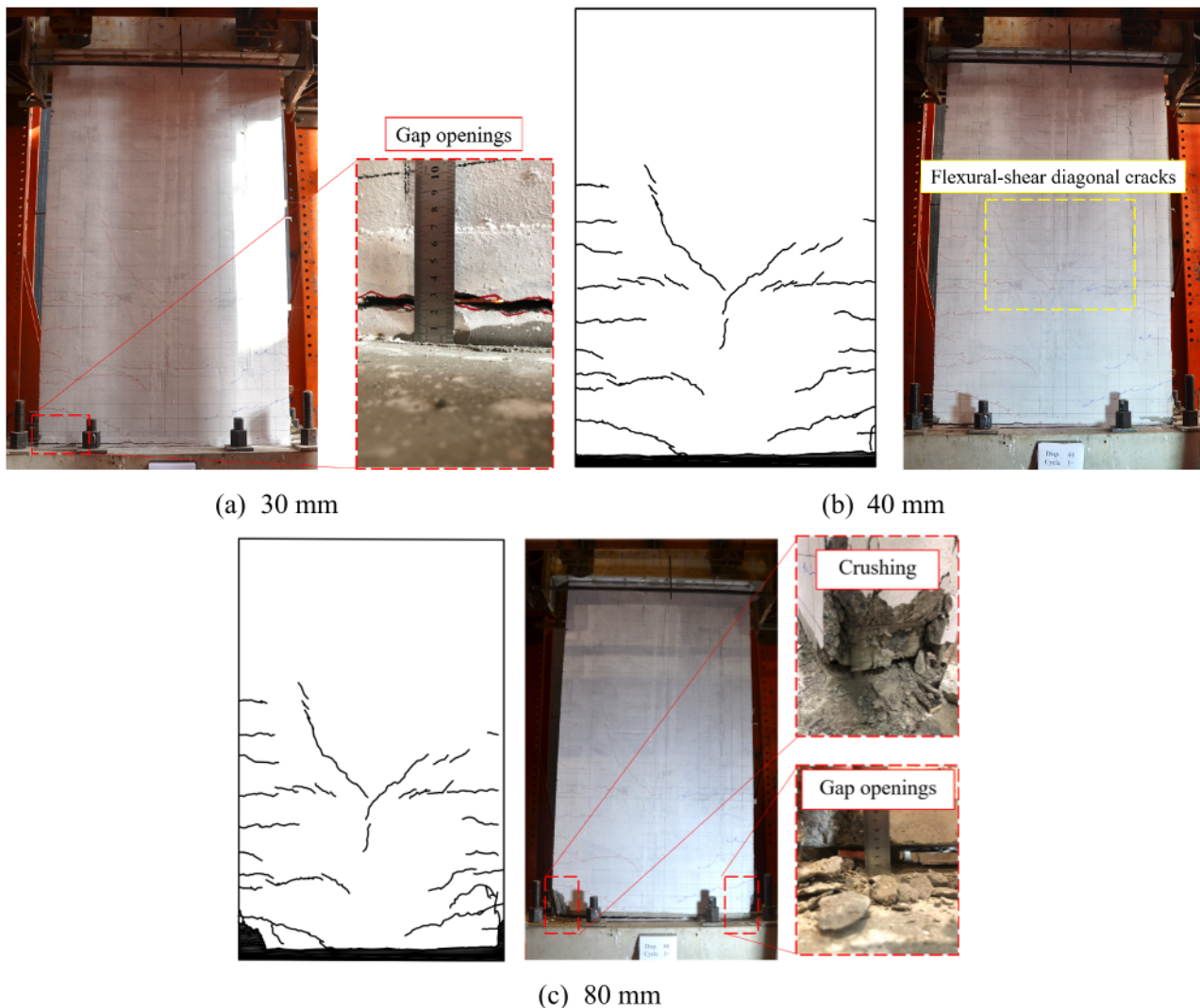


**Fig. 10.** Damage evolution of PSW2-60

- Unconfined concrete fiber
- Confined concrete fiber (boundary element)
- Confined concrete fiber (wall web)
- Reinforcing steel fiber

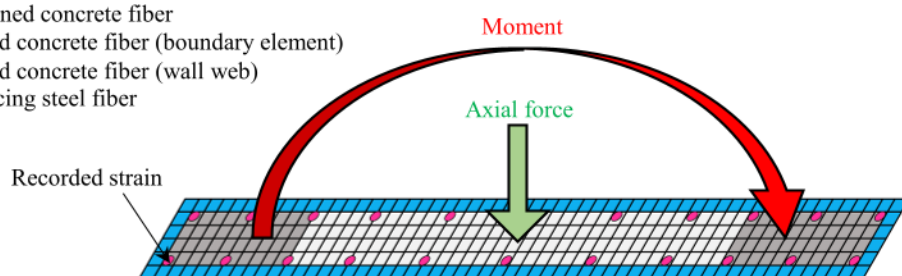


**Fig. 11.** Numerical model for the moment-curvature analysis

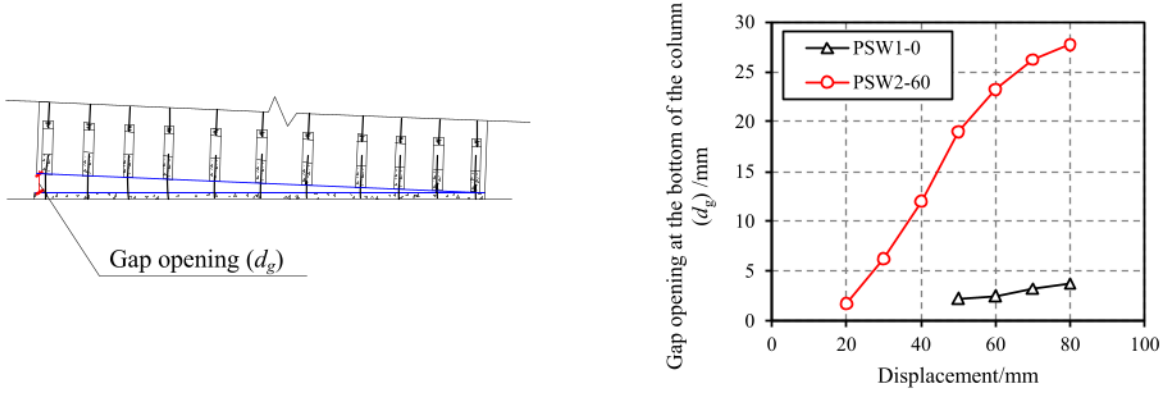
### *3.1.3 Comparison of failure modes*

By comparing PSW1-0 and PSW2-60, the differences in the critical damage characteristics between the PSWs with and without grouting defects were identified as follows:

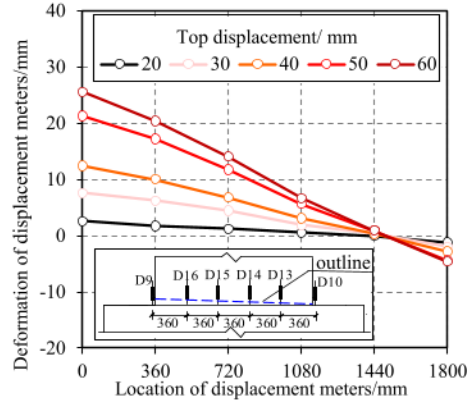
(1) Bar-slip characteristics of GSC: For the specimen without grouting defects, a negligible decrease in the strength was observed with an increase in the top displacement until the significant crushing of concrete and fracture of rebar. The sound caused by the anchorage failure of the grouting material in the GSCs and the unloading stiffness with a value of approximately zero was not observed. However, the strength of PSW2-60 significantly decreased since an obvious bar slip occurred at a top displacement of 20 mm. Furthermore, the unloading stiffness with a value of approximately zero became more obvious with the increase in the displacement amplitude. The average gap openings at the boundary of the PSWs with notable displacement amplitude are compared in Fig. 11a; the openings of PSW2-60 with grouting defects are significantly larger (approximately 7.5 times at 80 mm) than those of PSW1-0 without defects, which is attributed to the bar slip.

(2) Rocking behavior of PSW. A distinct rocking behavior was observed for specimen PSW2-60. The relative deformations between the bottom of the wall and the surface of the foundation in the positive loading direction were measured with six displacement meters, as shown in Fig. 11b. The largest deformation appears at the tension side of the shear wall, and it is notable that the measured deformations along the section of PSW2-60 are approximately linearly distributed and are much larger than those of PSW1-0. This phenomenon indicates that the rigid body rotation caused by the bar-slip phenomenon contributes a high percentage to the top deformation of PSW2-60, leading to the rocking phenomenon of such a specimen. In contrast, for PSW1-0, such rocking behavior was not observed because the bar slip phenomenon was prevented through sufficient grouting and the flexural behavior dominated the deformation mode of PSW1-0. It is noteworthy that because of the rocking behavior, the damage extent of PSW2-60 is relatively less severe than that of PSW1-0, as shown in Fig. 9 and Fig. 10. However, the ductility of PSW2-60 is lower than PSW1-0, detailed discussion can be found in Section 3.3.

(3) Damage characteristics of concrete: The damage region of PSW2-60, as shown in Fig. 10, caused by the compression of concrete, was much smaller than that of PSW1-0, as shown in Fig. 9. Meanwhile, the flexural-shear diagonal cracks at the web member of PSW2-60 were less than those of PSW1-0. The damage to concrete of PSW1-0 was significantly more severe than that of PSW2-60. Two characteristics may contribute to the decrease of concrete damage, the first is that the rocking phenomenon decreased the flexural and shear deformation of PSW2-60, the other is the lower horizontal load observed at the later loading stage for PSW2-60 after the occurrence of bar slip.



(a) Comparison of gap openings at the bottom of the specimens with and without defect



(b) Rocking behavior of PSW2-60 (positive loading)

**Fig. 11.** Deformation mode of the specimens with and without defect

### 3.2 Comparison of hysteretic responses

The horizontal load-displacement hysteretic curves of PSW1-0 and PSW2-60 are compared in Fig. 12.

(1) Before the top displacement reached 15 mm (corresponding to a drift ratio of 0.48%), the hysteretic responses of these two specimens were approximately identical and good energy dissipation capacities were observed.

(2) As the top displacement reached 20 mm (i.e., a drift ratio of 0.63%), owing to the further development of bar slip for PSW2-60, the strength of this specimen steadily decreased with the increase in top displacement, and the pinching phenomenon of the hysteretic curve became more obvious with the increase in top displacement. In contrast, the strength of PSW1-0 without grouting defects remained approximately stable before the top displacement reached 80 mm, and a pinching phenomenon was not exhibited, leading to a desirable energy dissipation capacity, which is the expected seismic performance. Such behavior is similar to the cast-in-place reinforced concrete shear walls.

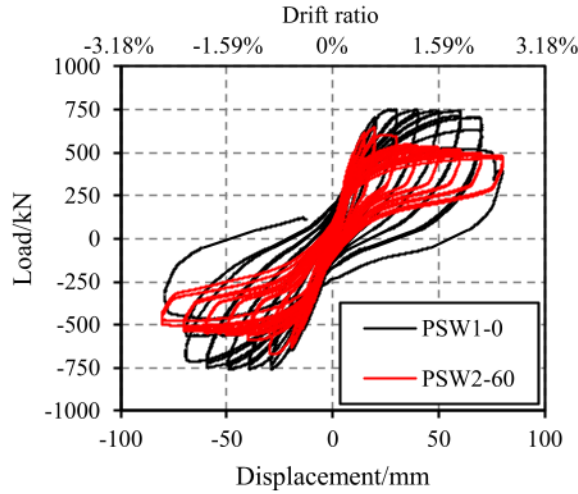


**Fig. 12.** Comparison on the load-displacement hysteretic curves of PSW1-0 and PSW2-60

### 3.3 Strength and deformation capacities

The skeleton curves of the two specimens are presented in Fig. 13. The yield point was determined according to [29], and the ultimate point was taken when the load decreased to 85% of the peak load. The characteristic points of skeleton curves of the two specimens are compared in Table 3. It can be found that:

(1) Yield point: The yield loads for the positive and negative directions of PSW2-60 were 14.7% and 9.0% lower than those of PSW1-0, respectively, indicating that the defect ratio of 60% has a certain influence on the yield load.

(2) Peak point: Because the bar slip occurred soon after the yielding of the longitudinal rebar, the loads and displacements of the peak points for PSW2-60 are also smaller than those of PSW1-0. Specifically, the defect ratio of 60% led to a decrease of in peak loads by 14.1% and 11.8% in the positive and negative directions, respectively. Meanwhile, this defect ratio caused a 31.4% and 1.4% decrease in the displacements associated with the peak load in the positive and negative directions, respectively.

(3) Ultimate point: The ultimate displacement of PSW1-0 with a value of approximately 71.9 mm is considerably larger than those of the specimen with defect, i.e., 38.9 mm and 46.2 mm for PSW2-60 at the positive and negative directions, respectively. The ductility ratio of PSW1-0 and PSW2-60 in the positive direction were 4.0 and 3.0, respectively. The values in the negative direction were 3.4 and 2.5, respectively. These results indicate that the deformation capacity and ductility of the specimen with grouting defects were significantly poorer than those of the specimen without grouting defects, and this was attributed to the bar-slip phenomenon.

Based on the above discussion, a defect ratio of 60% led to a significant decrease in the strength, deformation capacity and ductility of the PSW connected using GSC. In particular, the bar-slip phenomenon significantly decreased the ductility of the PSW.

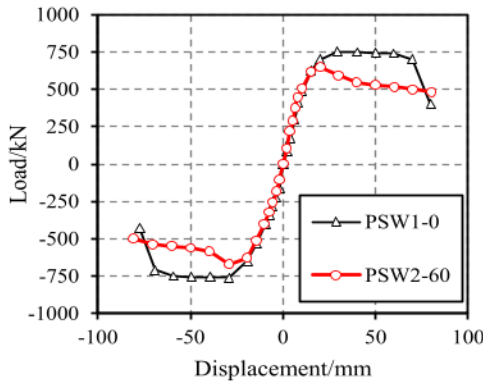


**Fig. 13.** Comparison on the skeleton curves of PSW1-0 and PSW2-60

**Table 3.** The parameters of characteristic points of skeleton curves of PSW1-0 and PSW2-60

Specimens	Loading direction	Yield point		Peak point		Ultimate point		Ductility ratio $\mu = \Delta_u / \Delta_y$
		$\Delta_y/\text{mm}$	$F_y/\text{kN}$	$\Delta_{\max}/\text{mm}$	$F_{\max}/\text{kN}$	$\Delta_u/\text{mm}$	$F_u/\text{kN}$	
PSW1-0	+	18.0	660.1	28.9	754.1	71.9	641.0	4.0
	-	-20.8	-667.8	-29.1	-762.3	-71.1	-648.0	3.4
PSW2-60	+	12.8	563.1	19.8	647.4	38.9	550.3	3.0
	-	-18.6	-608.0	-28.7	-672.2	-46.2	-571.4	2.5

Note:  $\Delta_y$  – displacement of the yield point,  $F_y$  – yield load,  $\Delta_{\max}$  – displacement of the peak point,  $F_{\max}$  – peak load,  $\Delta_u$  – displacement of the ultimate point,  $F_u$  – ultimate load

### 3.4 Stiffness degradation and energy dissipation capacities

Effective stiffness (i.e., average secant stiffness associated with each displacement amplitude) degradation curves of PSW1-0 and PSW2-60 are compared in Fig. 15. The initial elastic stiffnesses of these two PSWs were approximately identical, and the difference in effective stiffness between the two specimens was negligible, with a maximum relative difference of 5.1% before 15 mm. This is mainly due to that the bar-slip of sleeve connection with grouting defect occurred after the rebar yielded as shown in Fig. 2a. After the occurrence of bar slip (i.e., 20 mm), the effective stiffness of PSW2-60 rapidly decreased and was less than that of PSW1-0.

The cumulative hysteretic energy is a critical indicator for evaluating the seismic performance of the tested specimens. Hence, the energies at each displacement amplitude of the two specimens are compared in Fig. 15. The differences between the two specimens were considered negligible before the occurrence of bar slip. However, the energy dissipation capacity significantly decreased after the bar slip occurred for PSW2-60; the maximum difference reached 36.8% at the maximum top displacement.

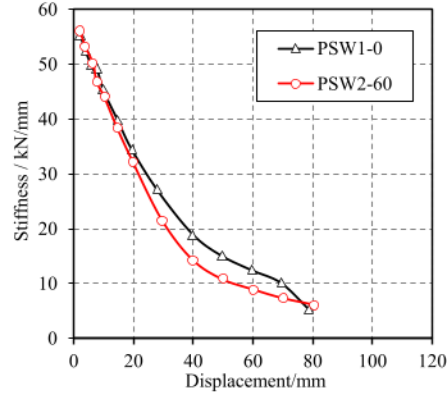


**Fig. 14.** Stiffness degradation of the specimens with and without defect

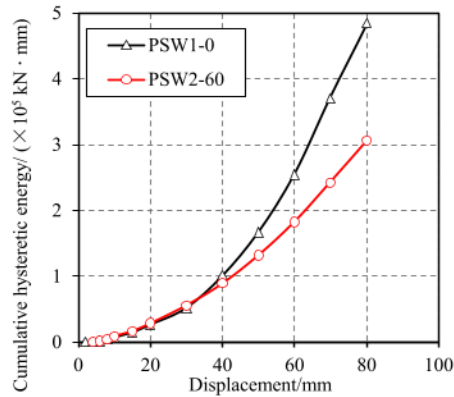


**Fig. 15.** Cumulative dissipated energy of the specimens with and without defect

#### 4 Comparison of the seismic performance of specimens before and after repair

##### 4.1 Failure modes of repaired specimens

###### 4.1.1 PSW3-60-R

For the repaired PSW with an initial defect ratio of 60% (i.e., PSW3-60-R), the expected flexural failure mode, instead of the bar-slip failure mode, was observed. Photographs of the critical damage states are presented in Fig. 16. The initial horizontal flexural crack was observed at the bottom of the PSW when the displacement reached 8 mm (i.e., a drift ratio of 0.254%). As this displacement approached 15 mm (i.e., a drift ratio of 0.476%), the longitudinal rebar yielded and the horizontal flexural crack pulled through. When the displacement reached approximately 30 mm (i.e., a drift ratio of 0.952%), the peak load was observed with a value of 763.3 kN associated with the spalling of cover concrete as shown in Fig. 16a, which is approximately identical to that of PSW1-0 (i.e., 754.1 kN).

At 40 mm (i.e., a drift ratio of 1.270%), numerous flexural-shear diagonal cracks, as shown in Fig. 16b, were developed and observed, which is similar to the phenomenon of PSW1-0 as shown in Fig. 9b. At 50 mm (i.e., a drift ratio of 1.587%), spalling of the cover concrete appeared within a height of 500 mm, and the gap opening was negligible at the boundary of the PSW.

When PSW3-60-R was firstly loaded to 60 mm (i.e., a drift ratio of 1.905%) in positive direction, significant concrete crushing in the compressive region and buckling of longitudinal rebars were observed, as shown in Fig. 16c, causing a significant decrease in the strength (approximately 19.7%). However, such a phenomenon

was not observed during the negative loading. Furthermore, at the second loading in the positive direction, the horizontal load further decreased to 460 kN, which is 60% of the peak load. Although these, a gap opening of 1.3 mm was observed at the boundary of PSW3-60-R. It is worth mentioning that the bar slip of PSW2-60 at 60 mm reached approximately 23.3 mm, which is significantly larger than that of PSW3-60-R, indicating that the bar slip was effectively controlled after the repair.

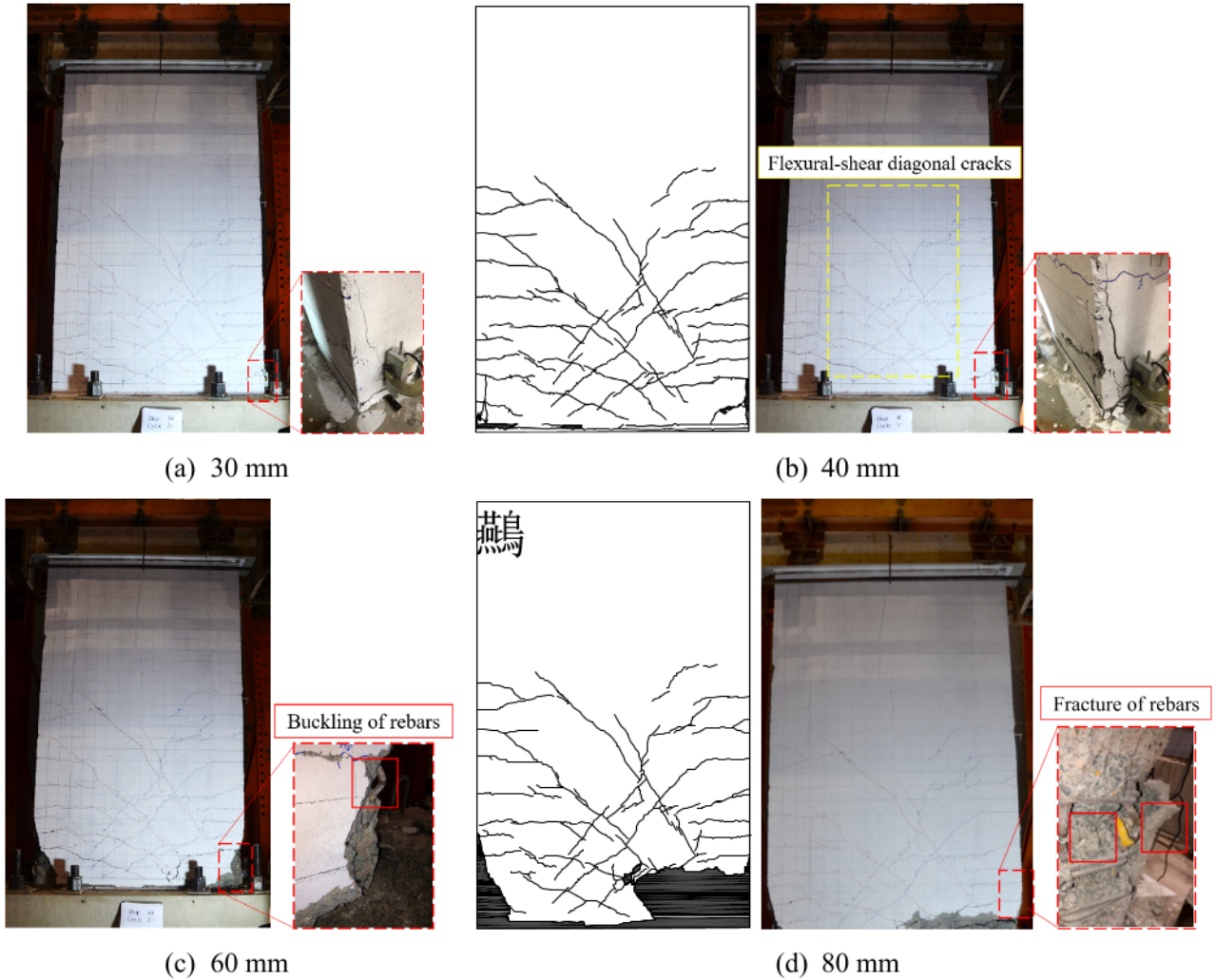


**Fig. 16.** Damage evolution of PSW3-60-R

When this specimen was loaded to 70 mm (i.e., a drift ratio of 2.222%), the concrete was crushed at the right side of the PSW with a width of about 700 mm in the compressive region and two longitudinal rebars fractured. The strength decreased to 40.8% of the peak load. Owing to the severe damage in the positive loading direction, the specimen was directly loaded to 80 mm (i.e., a drift ratio of 2.540%) in the negative direction and thereafter the test was end. The load steadily decreased to 82.6% of the peak load at this displacement, and less damage was observed for the concrete in the compressive region on the left side in comparison with that at the right side.

#### 4.1.3 Comparison of failure modes

By comparing the repaired specimen (i.e., PSW3-60-R), the corresponding specimen with grouting defects (i.e., PSW2-60), and the specimen without grouting defects (i.e., PSW1-0), the damage characteristics and

failure modes are as follows:

(1) Bar-slip characteristics of rebar in GSC: The deformation modes of PSW3-60-R are approximately identical to those of PSW1-0 before 60 mm (i.e., 1.9% drift ratio), and the bar slip was not observed during the test. The gap openings at the toe of the three PSWs are compared in Fig. 17. With the top displacement reached 80 mm, the average gap openings at the boundary of the PSW are 3.8 mm, 27.8 mm, and 1.8 mm for PSW1-0, PSW2-60, and PSW3-60-R, respectively. These results indicate that the bar slip was almost eliminated after the repair of insufficient grouting. It is noteworthy that the gap openings at the bottom of PSW2-60-R is lower than that of PSW1-0, this may be due to that the distribution of damage (i.e., cracking) of concrete components are usually random to some extent. In other words, although the overall damage extent of PSW1-0 and PSW2-60-R are quite similar, because of the randomness of cracking distribution, the flexural cracks of PSW1-0 are mainly concentrated at the bottom of shear wall, whereas for PSW2-60-R, the flexural cracks are mainly concentrated at the higher positions, leading to the measured gap openings of PSW2-60-R to be lower than that of PSW1-0.

(2) Damage characteristics of concrete: The flexural and flexural-shear cracks were fully developed for the repaired specimen, and the damage of concrete in the compressive region of PSW3-60-R was essentially identical to that of PSW1-0 before 60 mm, because the rocking phenomenon caused by the bar-slip characteristics is eliminated after repair. The fracture of the longitudinal rebar at 70 mm led to a certain difference in the damage of concrete in the compressive region. However, in comparison with the damage characteristics of PSW2-60, such a difference is not essential because it was not caused by the bar slip as in PSW2-60, it remained the typical flexural failure mode.

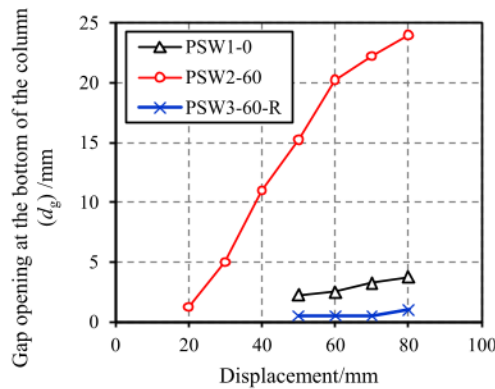


**Fig. 17.** Comparison of gap openings at the bottom of all specimens

#### 4.2 Comparison of hysteretic responses

The horizontal hysteretic curves of all the PSWs are compared in Fig. 18. It can be observed that:

(1) The pinching phenomenon, approximately zero unloading stiffness, and poor energy dissipation capacity of specimens with grouting defects were not observed for the repaired specimen. Good agreement was generally observed between the hysteretic curves of the repaired specimen and the specimen without grouting defects, indicating that a good energy dissipation capacity was realized after the repair.

(2) A certain extent of difference was observed between PSW1-0 and PSW3-60-R after the top displacement reached 60 mm (i.e., a 1.9% drift ratio). Specifically, a significant decrease in the strength was observed for

PSW3-60-R, which was caused by the fracture of the longitudinal rebar, which was not observed for PSW1-0 at this displacement. This difference may be due to the dispersion of the mechanical properties of the rebar, which is considered acceptable.

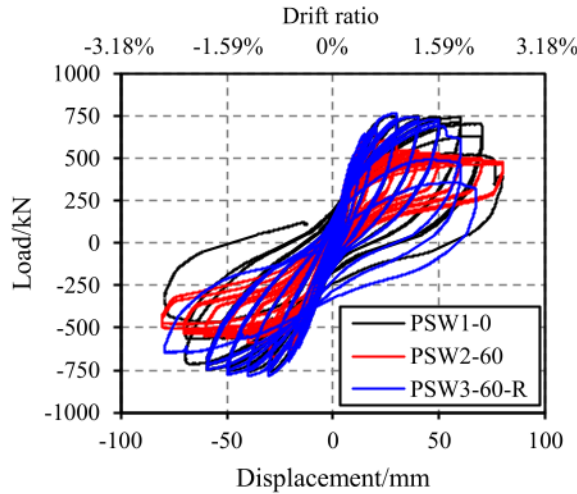


**Fig. 18.** Comparison on the load-displacement hysteretic curves of all specimens

#### 4.3 Strength and deformation capacity

The skeleton curves of the three PSWs are compared in Fig. 19. The characteristic points of skeleton curves of PSW1-0, PSW2-60, and PSW3-60-R are compared in Table 4.

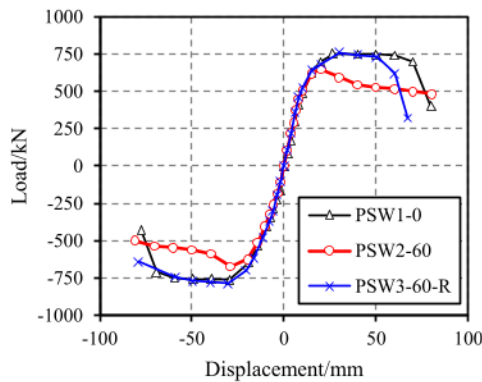


**Fig. 19.** Load-displacement skeleton curves of all specimens

**Table 4.** The parameters of characteristic points of skeleton curves of the specimens with and without defect

Specimens	Loading direction	Yield point		Peak point		Ultimate point		Ductility ratio $\mu = \Delta_u / \Delta_y$
		$\Delta_y/\text{mm}$	$F_y/\text{kN}$	$\Delta_{\max}/\text{mm}$	$F_{\max}/\text{kN}$	$\Delta_u/\text{mm}$	$F_u/\text{kN}$	
PSW1-0	+	18.0	660.1	28.9	754.1	71.9	641.0	4.0
	-	-20.8	-667.8	-29.1	-762.3	-71.1	-648.0	3.4
PSW2-60	+	12.8	563.1	19.8	647.4	38.9	550.3	3.0
	-	-18.6	-608.0	-28.7	-672.2	-46.2	-571.4	2.5
PSW3-60-R	+	16.8	651.9	28.5	763.3	57.3	648.8	3.4
	-	-20.4	-689.7	-29.9	-788.0	-73.6	-669.8	3.6

(1) Yield point: The relative differences between the yield loads of PSW1-0 and PSW3-60-R were no more than 3.3% and considered negligible. The relative differences in the yield displacements of PSW1-0 and

PSW3-60-R in the positive and negative directions were 6.7% and 1.9%, respectively, which were significantly smaller than those between PSW1-0 and the specimen with grouting defects.

(2) Peak point: The relative differences between the peak loads of PSW1-0 and PSW3-60-R were no more than 3.4% and were considered negligible. The relative differences in the displacements of the peak points were much smaller than those between PSW1-0 and PSW2-60.

(3) Ultimate point: The ultimate displacements of PSW3-60-R in the positive and negative directions are 57.3 mm and 73.6 mm, respectively. In the positive direction, the fracture of the longitudinal rebar led to a decrease in the deformation capacity and ductility of PSW3-60-R. Although it is a certain extent smaller than that of PSW1-0 (i.e., 71.9 mm), it was significantly larger than that of PSW2-60 without the repair (i.e., 38.9 mm). In contrast, the deformation capacity in the negative direction of PSW3-60-R was slightly better than that of PSW1-0, and was significantly better than that of PSW2-60 (i.e., 46.2 mm). As for the ductility, the ductility ratios of PSW3-60-R were 3.4 and 3.6 at the positive and negative directions, respectively, and are considered comparable with the specimen without defects (i.e., 4.0 and 3.4 for PSW1-0).

#### *4.4 Stiffness degradation and energy dissipation capacities*

The stiffness degradation and cumulative hysteretic energy curves of the three PSWs are compared in Figs. 20 and 21, respectively. After the repair of the grouting defect, the corresponding difference was significantly reduced. The stiffness degradation processes of the repaired specimen and the specimen without grouting defects are approximately identical. The cumulative hysteretic energies of PSW3-60-R were approximately identical to those of PSW1-0, with a maximum relative difference of 4.1%.

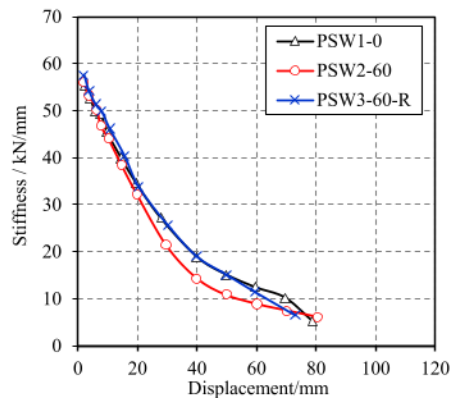


**Fig. 20.** Stiffness degradation of all specimens.

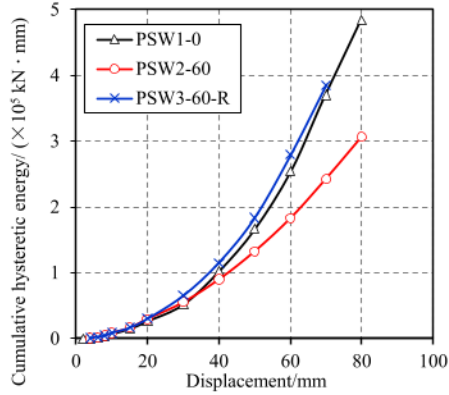


**Fig. 21.** Cumulative hysteretic energy of all specimens.

## 5 Conclusions

To investigate the effect of insufficient grouting on the seismic performance of PC shear walls using GSCs, and validate the feasibility and reliability of the repair method for insufficient grouting, three full-scale PSWs were tested under cyclic loads: one specimen without grouting defects, one specimen with a defect ratio of 60%, which was determined by the previously cyclic test results of GSCs with the identical longitudinal rebar, and one repaired specimen with an initial defect ratio of 60%. The effects of defect ratio and repair action were analyzed. The following conclusions were drawn.

(1) For the specimen with a defect ratio of 60%, the bar slip in GSCs occurred soon after the yielding of the longitudinal rebar and dominated the failure of the specimen as expected, rather than the flexural failure mode for the specimen without defects. A rocking phenomenon was observed for the deformation mode of the specimen since the occurrence of bar slip, thus leading to a pinching phenomenon for the corresponding hysteretic curves. The strength, deformation capacity, and energy-dissipation capacity were significantly lower than those of the specimen without defects. However, this deformation mode prevented the development of flexural-shear diagonal cracks and the concrete crushing in the compressive region, thus alleviating the damage to the concrete of the specimen with insufficient grouting.

(2) The bar-slip behavior was effectively prevented after the repair of insufficient grouting. Hence, the expected flexural failure mode was observed for the repaired PSW, and its strength, deformation capacity, and energy-dissipation capacity were comparable with those of the specimen without defects. Rocking behavior and pinching phenomenon were not observed after repair. The negative influences of insufficient grouting were almost eliminated, thus validating the feasibility and reliability of the repair method. The outcome of this study can serve as a reference for quality control of PC structures using GSCs.

## Acknowledgement

The authors are grateful for the financial support received from the National Key R&D Program of China (Grant No 2019YFE0112800) and the Pyramid Talent Training Project of Beijing University of Civil Engineering and Architecture (Grant No JDYC20200308).

## References

- [1] Henin E, Morcous G. Non-proprietary bar splice sleeve for precast concrete construction. Eng Struct

2015;83:154-62.

- [2] Xu GS, Wang Z, Wu B, Bursi OS, Tan XJ, Yang QB, et al. Seismic performance of precast shear wall with sleeves connection based on experimental and numerical studies. Eng Struct 2017;150:346-58.
- [3] Tullini N, Minghini F. Grouted sleeve connections used in precast reinforced concrete construction—Experimental investigation of a column-to-column joint. Eng Struct 2016;127:784-803.
- [4] Ameli MJ, Pantelides CP. Seismic analysis of precast concrete bridge columns connected with grouted splice sleeve connectors. J Struct Eng 2017;143:4016176.
- [5] Haber ZB, Saiidi MS, Sanders DH. Seismic performance of precast columns with mechanically spliced column-footing connections. Aci Struct J 2014;111:639-50.
- [6] Peng YY, Qian JR, Wang YH. Cyclic performance of precast concrete shear walls with a mortar-sleeve connection for longitudinal steel bars. Mater Struct 2016;49:2455-69.
- [7] Gu Q, Dong G, Wang X, Jiang HB, Peng SM. Research on pseudo-static cyclic tests of precast concrete shear walls with vertical rebar lapping in grout-filled constrained hole. Eng Struct 2019;189:396-410.
- [8] Wu M, Liu X, Liu HT, Du XL. Seismic performance of precast short-leg shear wall using a grouting sleeve connection. Eng Struct 2020;208:110338.
- [9] Xiao S, Wang ZL, Li XM, Harries KA, Xu QF, Gao RD. Study of effects of sleeve grouting defects on the seismic performance of precast concrete shear walls. Eng Struct 2021;236:111833.
- [10] Ling JH, Rahman ABA, Ibrahim IS, Hamid ZA. Behaviour of grouted pipe splice under incremental tensile load. Constr Build Mater 2012;33:90-8.
- [11] Seo SY, Nam BR, Kim SK. Tensile strength of the grout-filled head-splice-sleeve. Constr Build Mater 2016;124:155-66.
- [12] Kahama EK, Xie FZ, M. Anglaaere DL. Numerical study on the influence of defects in grouting on the mechanical properties of a full grouted sleeve connector. J Adhesion 2021;1-32.
- [13] Lu ZW, Huang J, Li YB, Dai SB, Peng Z, Liu X, et al. Mechanical behaviour of grouted sleeve splice under uniaxial tensile loading. Eng Struct 2019;186:421-35.
- [14] Ling JH, Rahman ABA, Ibrahim IS. Feasibility study of grouted splice connector under tensile load. Constr Build Mater 2014;50:530-9.
- [15] Chen XD. Performance of reinforced sleeve grouting joints under high stress cyclic loading. J Chongqing Univ Sci Technol: Nat Sci Ed 2020;22(1):110-3. (in Chinese)
- [16] Zheng GY, Kuang ZP, Xiao JZ, Pan ZF. Mechanical performance for defective and repaired grouted sleeve connections under uniaxial and cyclic loadings. Constr Build Mater 2020;233:117233.
- [17] Kuang ZP, Zheng GY, Jiao XT. Experimental study on effect of mechanical behavior of grout sleeve splicing for reinforced bars due to lack of grout. J Tongji Univ: Nat Sci Ed 2019;47:946-56. (in Chinese)
- [18] Chen X, Miao QS, Yang CT, Ge DD, Liu QM, Xie LL. Experimental study on tensile performance of defect detectable and repairable half grouted sleeve connection. Eng Mech 2020;37:199-207. (in Chinese)
- [19] Xie LL, Zhong BJ, Chen X, et al. Experimental investigation on the connection performance of defect

- detectable and repairable half-grouted sleeve under cyclic loads. *Concr Build Mater*, 2022, 323: 126593.
- [20] Li XM, Gao RD, Xu QF, Wang ZL, Zhang FW, Xie Y. Study on inspection technology for sleeve grouting connection quality of precast shear wall based on X-ray digital radiography method. *Build Struct* 2018;48:57-61. (in Chinese)
- [21] Feng K, Zhao Q, Qiu YP. Damage imaging in mesoscale concrete modeling based on the ultrasonic time-reversal technique. *Acta Mech Solida Sin* 2020;33:61-70.
- [22] Cao ZJ, Li QW. Effect of connection deficiency on seismic performance of precast concrete shear wall-frame structures. *J Earthq Tsunami* 2019;13:1940005.
- [23] MOHURD (Ministry of Housing and Urban-rural Development). Technical Specification for Grout Sleeve Splicing of Rebars (JGJ355-2015). China Architecture & Building Press Beijing, China 2015. (in Chinese)
- [24] Waygate Technologies. Mentor Visual iQTM, from <https://www.bakerhughesds.com/remote-visual-inspection/video-borescopes/mentor-visual-iq-3d-videoscope/>; 2021.
- [25] MOHURD (Ministry of Housing and Urban-rural Development). Cementitious grout for sleeve of rebar splicing (JG/T 408-2019). China Architecture & Building Press Beijing, China 2019. (in Chinese)
- [26] FEMA 461 Interim testing protocols for determining the seismic performance characteristics of structural and nonstructural components. Federal Emergency Management Agency (FEMA); 2007.
- [27] F. Mckenna, OpenSees: a framework for earthquake engineering simulation, *Comput. Sci. Eng.* 13 (2011) 58–66.
- [28] D.C. Kent, R. Park, Flexural members with confined concrete, *J. Struct. Div.* 97 (1971) 1969–1990.
- [29] Park R. Evaluation of ductility of structures and structural assemblages from laboratory testing. *Bull N Z Soc Earth* 1989;22:155-66.